



# CHORUS

This is the accepted manuscript made available via CHORUS. The article has been published as:

## Electrically tunable transport and high-frequency dynamics in antiferromagnetic $\text{Sr}_{\{3\}}\text{Ir}_{\{2\}}\text{O}_{\{7\}}$

Heidi Seinige, Morgan Williamson, Shida Shen, Cheng Wang, Gang Cao, Jianshi Zhou, John B. Goodenough, and Maxim Tsoi

Phys. Rev. B **94**, 214434 — Published 29 December 2016

DOI: [10.1103/PhysRevB.94.214434](https://doi.org/10.1103/PhysRevB.94.214434)

# Electrically tunable transport and high-frequency dynamics in antiferromagnetic $\text{Sr}_3\text{Ir}_2\text{O}_7$

Heidi Seinige<sup>1,2</sup>, Morgan Williamson<sup>1,2</sup>, Shida Shen<sup>1,2</sup>, Cheng Wang<sup>1,2</sup>, Gang Cao<sup>3,4</sup>, Jianshi Zhou<sup>2</sup>, John B. Goodenough<sup>2</sup>, Maxim Tsoi<sup>1,2</sup>

<sup>1</sup>*Physics Department, The University of Texas at Austin, Austin, Texas 78712, USA*

<sup>2</sup>*Texas Materials Institute, The University of Texas at Austin, Austin, Texas 78712, USA*

<sup>3</sup>*Department of Physics, University of Colorado-Boulder, Boulder, CO 80309, USA*

<sup>4</sup>*Center for Advanced Materials, University of Kentucky, Lexington, Kentucky 40506, USA*

## ABSTRACT

We report dc and high-frequency transport properties of antiferromagnetic  $\text{Sr}_3\text{Ir}_2\text{O}_7$ . Temperature-dependent resistivity measurements show that the activation energy of this material can be tuned by an applied dc electrical bias. The latter allows for continuous variations in the sample resistivity of as much as 50% followed by a reversible resistive switching at higher biases. Such a switching is of high interest for antiferromagnetic applications in high-speed memory devices. Interestingly, we found the switching behavior to be strongly affected by a high-frequency (microwave) current applied to the sample. The microwaves at 3-7 GHz suppress the dc switching and produce resonance-like features that we tentatively associated with the dissipationless magnonics recently predicted to occur in antiferromagnetic insulators subject to ac electric fields. We have characterized the effects of microwave irradiation on electronic transport in  $\text{Sr}_3\text{Ir}_2\text{O}_7$  as a function of microwave frequency and power, strength and direction of external magnetic field, strength and polarity of applied dc bias, and temperature. Our observations support the potential of antiferromagnetic materials for high-speed/high-frequency spintronic applications.

Antiferromagnetic (AFM) spintronics is one of many promising routes for ‘beyond the CMOS’ technologies where unique properties of AFM materials are explored to achieve new and improved functionalities. AFMs are especially interesting for high-speed memory applications thanks to their high natural frequencies. Of particular interest are 5-d transition metal oxides (TMO) due to their rich and widely unexplored physical phenomena. In these systems, comparable energy scales of crystal-field splitting, electron correlations, and spin-orbit coupling (SOC) result in close interconnections between physical properties and crystal structure. For instance, a very large anisotropic magnetoresistance (AMR) [1] and reversible resistive switching driven by high-density currents/high electric fields [2] were both demonstrated in an AFM Mott insulator  $\text{Sr}_2\text{IrO}_4$ . These results provide an interesting insight into using such phenomena for writing and reading information in spintronic memory applications, but the relatively low Néel temperature of  $\text{Sr}_2\text{IrO}_4$  ( $T_N=240$  K) makes this specific material impractical. Further studies of such materials are, however, in demand as recent experimental [3, 4] and theoretical [5, 6, 7] results have indicated a possibility of superfluid spin transport in AFM insulators that may open up a completely new pathway to transfer information in AFM spintronic devices.

In this letter we study electrical transport properties of  $\text{Sr}_3\text{Ir}_2\text{O}_7$  – a sister compound to  $\text{Sr}_2\text{IrO}_4$  [8] – with a higher Néel temperature ( $T_N=285$  K). Temperature-dependent resistivity measurements show that the activation energy in this new compound depends on the applied dc electrical bias but with little or no dependence on the applied magnetic field. This bias dependence allows to drive continuous variations in the sample resistivity by as much as 50% followed by a reversible resistive switching at higher biases. Such a switching may potentially be used for the writing operation in memory devices based on AFMs; high precession frequencies associated with AFMs make them ideal candidates for future high-speed memory applications. While our dc resistivity measurements confirm the potential of iridates for such applications, the main interest lies in probing their high-frequency properties. That is just what we did with our present experiments. We observed that the switching behavior in antiferromagnetic  $\text{Sr}_3\text{Ir}_2\text{O}_7$  is strongly affected by a high-frequency (microwave) current applied to the sample. The microwaves at 3-7 GHz produce resonance-like features at higher biases that may be tentatively associated with the dissipationless magnonics recently predicted [6] to occur in AFM insulators in the presence of an ac electric field. We have characterized the effects of high-frequency radiation on electronic transport in  $\text{Sr}_3\text{Ir}_2\text{O}_7$  as a

function of microwave power and frequency, strength and direction of externally applied magnetic field, temperature, and strength and polarity of a dc bias.

In our experiments we used single crystals of  $\text{Sr}_3\text{Ir}_2\text{O}_7$  synthesized via a self-flux technique described elsewhere [9]. The technique results in single crystalline flakes of  $\text{Sr}_3\text{Ir}_2\text{O}_7$  with thickness of about 0.2-mm and the [001]  $c$ -axis oriented perpendicular to the flake's surface (area  $\sim 0.5 \times 0.5 \text{ mm}^2$ ). The crystal structure of the flakes was determined by single crystal X-ray diffraction. Ag and In metal contacts (area  $\sim 0.2 \times 0.2 \text{ mm}^2$ ) on the top and bottom surfaces of the  $\text{Sr}_3\text{Ir}_2\text{O}_7$  flakes were used to supply and sink electrical currents; dc (up to 50 mA) and rf (2-7 GHz) currents were combined with a bias tee. In such a 2-probe geometry, the applied currents flow (primarily) along the [001]  $c$ -axis of the crystal; 4-probe measurements were also performed (with two extra metal contacts) to verify that the observed effects are not related to metal/semiconductor contacts. In magnetic fields (up to 250 mT) applied parallel and perpendicular to the [001]  $c$ -axis and at temperatures from 77 to 300 K we have characterized: (i) the dc transport properties of  $\text{Sr}_3\text{Ir}_2\text{O}_7$  by performing temperature-dependent resistivity and current-voltage ( $I$ - $V$ ) measurements and (ii) the high-frequency transport in  $\text{Sr}_3\text{Ir}_2\text{O}_7$  via a heterodyne detection scheme like the one used for electrical detection of ferromagnetic resonance [10]. Here the high-frequency response is monitored by detecting a small rectification voltage  $V_\omega$ , which appears across the sample at resonance, while the applied microwave current is amplitude-modulated and a lock-in amplifier is used for  $V_\omega$  detection to increase the signal-to-noise ratio.

Figure 1a shows the temperature dependence of  $\text{Sr}_3\text{Ir}_2\text{O}_7$  resistance at a small bias ( $I = 0.1 \text{ mA}$ ); the inset shows the corresponding Arrhenius plot –  $\ln(R)$  vs  $1/T$ . From the plot's slope we extracted (Fig. 1b) the activation energy ( $\Delta_0 \approx 30\text{-}60 \text{ meV}$  for  $T=77\text{-}200 \text{ K}$ ) which turns out to be on average slightly lower than in  $\text{Sr}_2\text{IrO}_4$  [2] but agrees reasonably well with the values found in  $\text{Sr}_3\text{Ir}_2\text{O}_7$  via optical methods [11]. By performing a similar analysis at different applied bias currents  $I$  we were able to reconstruct the bias dependence of the activation energy  $\Delta_0$  at a fixed temperature. Figure 1c shows an example of such a reconstruction  $\Delta_0$  vs  $I$  at  $T = 176 \text{ K}$ ; similar results were found at different temperatures. The activation energy is found to decrease with an applied electric bias similar to the behavior observed previously in  $\text{Sr}_2\text{IrO}_4$  [2]. In the case of  $\text{Sr}_2\text{IrO}_4$  the decrease of the activation energy has been attributed to electric-field-induced lattice distortions and their effect on electronic states and transport properties. High local electric fields in our experiments alter the

equilibrium positions of oxygen with respect to iridium ions and induce distortions of the corner shared  $\text{IrO}_6$  octahedra, thus, provoking modifications of the localized states and electronic structure. The displacements of oxygen ions are expected to be along the applied electric field, i.e. along the  $c$ -axis, and estimated [2] to be  $\sim 2 \cdot 10^{-3}$  Å ( $\sim 0.1$  % of the Ir-O bond length). We have verified such a field effect in  $\text{Sr}_3\text{Ir}_2\text{O}_7$  by measuring current-voltage ( $I$ - $V$ ) characteristics at different temperatures. Figure 2 shows the experimental dependence of  $\text{Sr}_3\text{Ir}_2\text{O}_7$  resistance  $R=V/I$  on the bias current  $I$  at different temperatures from 87-180 K (open symbols). Solid curves are fits to each  $R(I)$  using the field-effect model [2]:

$$R(I) = A * e^{\Delta(I)/2k_B T}, \quad \Delta(I) = \Delta_0 - B * |I| \quad (1)$$

where  $\Delta_0$  is the thermal activation energy at zero bias for a given temperature extracted from Fig. 1b, and  $A$  and  $B$  are fitting parameters (see insets to Fig. 2):  $A$  is related to intrinsic properties of the material and scales with  $\Delta_0$  and  $T$ ;  $B$  characterizes the strength of the field effect and found to decrease with  $T$  in both  $\text{Sr}_2\text{IrO}_4$  and  $\text{Sr}_3\text{Ir}_2\text{O}_7$ . In addition to the field effect, we tested other models typically used for explaining non-linear  $I$ - $V$  characteristics in semiconductors but found systematic discrepancies between their predictions and observed curves (see Supplemental Material) [11]. We thus conclude that the dc transport properties of  $\text{Sr}_3\text{Ir}_2\text{O}_7$  can be best described by the field-effect model (Eq. 1).

We have demonstrated previously in  $\text{Sr}_2\text{IrO}_4$  [2] a reversible resistive switching that could be associated with a bias-induced structural transition between two metastable states. Figure 3a shows similar switching events observed in  $R(I)$  characteristics of  $\text{Sr}_3\text{Ir}_2\text{O}_7$ . Here the black and grey curves show the  $R(I)$  for up- and down-sweeps of the applied  $I$ . In the case of  $\text{Sr}_3\text{Ir}_2\text{O}_7$  we observe multiple switching events at high bias currents above some critical value ( $|I_C|$ ). It is important to note that the switching depends on the history of electric-bias sweeping: going up from zero bias the system remains in a ‘low-resistance’ state (grey curve) up to a critical bias ( $I_C \approx 12$  mA) at which the switching to a ‘high-resistance’ state occurs; going down from a high positive bias the resistance remains in the ‘high-resistance’ state (black curve) to well below  $I_C$ , and then gradually merges the ‘low-resistance’ state at around 5 mA. In contrast to  $\text{Sr}_2\text{IrO}_4$ , where an increasing bias promotes a switching from ‘high’ to ‘low’ resistance, the switching observed in  $\text{Sr}_3\text{Ir}_2\text{O}_7$  is from ‘low’ to ‘high’ state. This difference can be related to different magnetic structures of  $\text{Sr}_2\text{IrO}_4$  and  $\text{Sr}_3\text{Ir}_2\text{O}_7$ : while

$\text{Sr}_2\text{IrO}_4$  exhibits a weak ferromagnetism arising from canted antiferromagnetic moments in the ab-basal plane [13],  $\text{Sr}_3\text{Ir}_2\text{O}_7$  has a c-axis collinear antiferromagnetic structure without any spin-canting component [11, 14-16]. Note that the switching was observed only at temperatures close to 77 K and disappears above 100 K. Also we did not find any effects of externally applied magnetic field on the dc transport in  $\text{Sr}_3\text{Ir}_2\text{O}_7$ . Unlike  $\text{Sr}_2\text{IrO}_4$ , which displayed both (anisotropic) magnetoresistance (MR) and corresponding variations in  $I_C$  correlated with MR [2],  $\text{Sr}_3\text{Ir}_2\text{O}_7$  shows neither a field-dependence of the critical current (Fig. 3b) nor MR (Fig. 3c). This zero magnetotransport response can also be related to the collinear (c-axis) antiferromagnetic structure in  $\text{Sr}_3\text{Ir}_2\text{O}_7$ , which is much less responsive to an external magnetic field compared to the canted ab-plane antiferromagnetic moments in  $\text{Sr}_2\text{IrO}_4$ .

Next we probe the response of  $\text{Sr}_3\text{Ir}_2\text{O}_7$  to high frequencies – in addition to a dc bias we apply a microwave current (in the frequency range from 2-7 GHz). In this set of measurements we are using a different (slightly bigger) flake of  $\text{Sr}_3\text{Ir}_2\text{O}_7$  compared to that used in Figs. 1-3. All high-frequency measurements were done at  $T=77$  K. The effect of microwaves is monitored by (1) tracking changes in the  $R(I)$  characteristics and by (2) detecting a small rectification voltage  $V_\omega$  induced in  $\text{Sr}_3\text{Ir}_2\text{O}_7$  by microwaves. The latter is a standard method for detecting high-frequency magnetodynamics in ferromagnetic systems; the applied microwave current is amplitude-modulated and  $V_\omega(I)$  is measured by a lock-in amplifier tuned to the modulation frequency. Figures 4-6 present detailed measurements of  $V_\omega(I)$  and  $R(I)$  under microwaves of 3 GHz with up to 20 dBm of power  $P$  at the output of microwave generator. Note that the actual power reaching the sample is significantly lower due to an impedance mismatch at the sample connections. We estimate the amplitude of the microwave current at the sample position as 1 mA for a 20 dBm generator power output.

Figure 4 shows a side-by-side comparison of  $V_\omega(I)$  (left) and  $R(I)$  (right) for low (-20 dBm – panels a and b), intermediate (10 dBm – panels c and d), and high (20 dBm – panels e and f) microwave power levels  $P_s$ . Gray and black traces represent up- and down-sweeps of  $I$ , respectively. At  $P = -20$  dBm (Fig. 4a-b),  $R(I)$  reveals a reversible resistive switching like the one discussed above (Fig. 3) while  $V_\omega(I)$  shows only a noise floor of less than 10  $\mu\text{V}$  which suddenly increases to more than 50  $\mu\text{V}$  above  $I_C = \pm 30$  mA. The microwave signal applied to the sample at  $P = -20$  dBm is negligible, so these results are identical to measurements with no microwaves applied.

The increased noise above  $|I_C|$  may be an evidence of a fast but small resistive switching events which occur at higher biases. At  $P = 10$  dBm (Fig. 4c-d), the reversible resistive switching at  $I_C = \pm 30$  mA disappears (except for smaller jumps in  $R$ ) and the rectification  $V_\omega(I)$  signal emerges. Note that the  $V_\omega(I)$  signal preserves the hysteretic behavior of resistive switching observed without microwaves (compare up- and down-sweeps in Fig. 4c). At positive current biases in the gray up-sweep (negative in the black down-sweep) we observe a resonance-like structure at about  $\pm 20$  mA. Finally, at  $P = 20$  dBm (Fig. 4e-f), the resonance-like structure disappears and the overall shapes of  $V_\omega(I)$  and  $R(I)$  appear somewhat smeared out, which is not surprising given an inevitable averaging of dc signals at high amplitudes of applied ac (microwaves).

Figures 5a and 5b show detailed measurements of the power-dependence of  $R(I)$  and  $V_\omega(I)$ , respectively, from  $P = 0$ -19 dBm in 1 dBm steps. Only down-sweeps shifted vertically are shown here for clarity. The noise in  $R(I)$  around zero bias ( $I < 5$  mA) is due to the division ( $R=V/I$ ) by small  $I$ s. Up to 8 dBm the  $R(I)$  curves show a distinct switching behavior, which disappears at a critical power  $P_c=9$  dBm where the resonance-like structure at about -20 mA emerges in  $V_\omega(I)$ . An abrupt disappearance of the switching and onset of the resonance-like structure at  $P_c$  was verified with the smallest power step available (0.1 dBm). At higher power levels, the resonance-like structure broadens and shifts to a lower bias current as illustrated in Fig. 6. Here a 2D gray-density plot shows the rectification voltage  $V_\omega$  as a function of  $I$  and  $P$  with brighter color indicating a higher  $V_\omega$ . Several resonance-like peaks (at  $I = -19.5, -23.5, -27.5$  and  $-30$  mA) are visible. The critical power  $P_c$  where the structure emerges was found to decrease approximately linearly with increasing frequency of applied microwaves (inset to Fig. 5b). This observation unambiguously demonstrates that GHz radiation can affect the transport properties of antiferromagnets (without any presence of ferromagnets).

From X-ray resonant scattering, it is known that  $\text{Sr}_3\text{Ir}_2\text{O}_7$  has an antiferromagnetic ground state with the antiferromagnetic spin axis directed along the c-axis [14, 15]. It seems therefore natural to assume that antiferromagnetic resonance (AFMR) can be excited in our  $\text{Sr}_3\text{Ir}_2\text{O}_7$  samples. According to Kittel [17], AFMR is described by  $\omega/\gamma = H_0 \pm \sqrt{2H_A H_E}$ , where  $H_0$  is the applied magnetic field,  $H_A$  the anisotropy field,  $H_E$  the exchange field, and  $\gamma$  the gyromagnetic ratio. Assuming unreasonably low values of  $H_E \sim 10$  T and  $H_A \sim 0.1$  T  $\ll H_E$  we estimate an AFMR

frequency of  $\approx 40$  GHz at zero applied field (inaccessible in our experiments). However, we observed a resonance-like structure at much smaller frequency and with no frequency or magnetic field dependence [11] expected for AFMR. We thus conclude that our observations depicted in Figs. 4-6 are unlikely to be related to AFMR and suggest another mechanism based on a recent prediction of dissipationless spin currents in AFM insulators driven by ac electric fields [6].

A highly efficient transfer of spin currents across an antiferromagnetic NiO has been recently observed in YIG/NiO/Pt trilayers [3, 4]. Two different mechanisms have been proposed to explain the spin transport across an antiferromagnet: a non-equilibrium superfluid spin transport [5] and propagation of evanescent spin waves [18]. Note that in both cases a ferromagnetic material (YIG in Refs. 3, 4) ought to be present for generation of spin current. In contrast, Chen and Sigrist argued [6] that an oscillating electric field can alone excite spin currents in antiferromagnetic insulators even in the absence of ferromagnets. According to their predictions [6] no external magnetic field is required for the excitation, and dissipationless spin currents can be triggered via the magnetoelectric effect even when the oscillation frequency does not match the antiferromagnet's natural (AFMR) frequency. These predictions correlate well with our observations in the antiferromagnetic  $\text{Sr}_3\text{Ir}_2\text{O}_7$  without a ferromagnet – a resonance-like structure in  $V_{\omega}(I)$  is observed in a wide frequency range (from 2-5 GHz), independent of magnetic field, and depends on the applied electric field bias. According to Chen and Sigrist [6] dissipationless magnonics can be excited in multiferroic insulators with a coplanar AFM spiral order by oscillating electric fields. In  $\text{Sr}_3\text{Ir}_2\text{O}_7$  such an order may be initiated via the field effect: an applied dc bias leads to lattice distortions and associated electric polarization [2]; the lattice distortions, in turn, may alter the magnetic structure of  $\text{Sr}_3\text{Ir}_2\text{O}_7$  via spin-orbit coupling and promote a spiral-like AFM magnetic order at a certain level of applied dc bias ( $|I_C|$ ); finally, a sufficiently high ac current applied on top of the dc bias could excite the spin super currents. The absence of the switching in dc  $R(I)$  characteristics above this critical ac (microwave) power may be tentatively associated with the dissipationless nature of these excitations.

In summary, we have studied dc and high-frequency transport properties in antiferromagnetic  $\text{Sr}_3\text{Ir}_2\text{O}_7$ . Temperature-dependent resistivity and current-voltage ( $I$ - $V$ ) measurements showed an electrically tunable transport in  $\text{Sr}_3\text{Ir}_2\text{O}_7$  that can be successfully described by the field-effect model as was previously observed in  $\text{Sr}_2\text{IrO}_4$  [2]. The activation energy can be tuned by an applied dc electrical bias, which allows for a continuous variation of its resistivity by as much as 50% followed

by a reversible resistive switching at higher biases. The switching behavior is strongly affected by a high-frequency current applied to the sample. The microwaves (2-7 GHz) were found to suppress the dc switching and produce a resonance-like structure that we tentatively associate with dissipationless magnonics recently predicted to occur in antiferromagnetic insulators subject to ac electric fields. The critical power where the resonance-like structure emerges was found to decrease approximately linearly with increasing frequency of applied microwaves. This observation unambiguously demonstrates that GHz radiation can affect the transport properties of antiferromagnets without any involvement of ferromagnets. These findings are of high interest for future antiferromagnetic spintronics and spin dynamics with the goal of high-speed applications controlled by electric fields.

This work was supported in part by C-SPIN, one of six centers of STARnet, a Semiconductor Research Corporation program, sponsored by MARCO and DARPA, by NSF grants DMR-1207577, DMR-1265162, DMR-1600057, and DMR-1122603, and by the King Abdullah University of Science and Technology (KAUST) Office of Sponsored Research (OSR) under Award No. OSR-2015-CRG4-2626.

## References:

- [1] C. Wang, H. Seinige, G. Cao, J.-S. Zhou, J. B. Goodenough, and M. Tsoi, *Phys. Rev. X* **4**, 041034 (2014).
- [2] C. Wang, H. Seinige, G. Cao, J.-S. Zhou, J. B. Goodenough, and M. Tsoi, *Phys. Rev. B* **92**, 115136 (2015).
- [3] C. Hahn, G. de Loubens, V. V. Naletov, J. B. Youssef, O. Klein and M. Viret, *Europhys. Lett.* **108**, 57005 (2014).
- [4] H. Wang, C. Du, P. C. Hammel, and F. Yang, *Phys. Rev. Lett.* **113**, 097202 (2014).
- [5] S. Takei, B. I. Halperin, A. Yacoby, and Y. Tserkovnyak, *Phys. Rev. B* **90**, 094408 (2014).
- [6] W. Chen and M. Sigrist, *Phys. Rev. Lett.* **114**, 157203 (2015).
- [7] S. Takei, T. Moriyama, T. Ono, and Y. Tserkovnyak, *Phys. Rev. B* **92**, 020409(R) (2015).
- [8] B. J. Kim, H. Ohsumi, T. Komesu, S. Sakai, T. Morita, H. Takagi, T. Arima, *Science* **323**, 1329 (2009).
- [9] G. Cao, Y. Xin, C. S. Alexander, J. E. Crow, P. Schlottmann, M. K. Crawford, R. L. Harlow, and W. Marshall, *Phys. Rev. B* **66**, 214412 (2002).
- [10] H. Seinige, C. Wang, and M. Tsoi, *J. Appl. Phys.* **115**, 17D116 (2014).
- [11] See Supplemental Material at [link] for the crystal structure, alternative current-voltage models, and frequency and magnetic field dependent measurements.
- [12] H. J. Park, C. H. Sohn, D. W. Jeong, G. Cao, K. W. Kim, S. J. Moon, Hosub Jin, Deok-Yong Cho, and T. W. Noh, *Phys. Rev. B* **89**, 155115 (2014).
- [13] F. Ye, S. Chi, B. C. Chakoumakos, J. A. Fernandez-Baca, T. Qi, and G. Cao, *Phys. Rev. B* **87**, 140406(R) (2013).
- [14] S. Boseggia, R. Springell, H. C. Walker, A. T. Boothroyd, D. Prabhakaran, D. Wermeille, L. Bouchenoire, S. P. Collins, and D. F. McMorrow, *Phys. Rev. B* **85**, 184432 (2012).
- [15] J. W. Kim, Y. Choi, Jungho Kim, J. F. Mitchell, G. Jackeli, M. Daghofer, J. van den Brink, G. Khaliullin, and B. J. Kim, *Phys. Rev. Lett.* **109**, 037204 (2012).
- [16] S. Boseggia, R. Springell, H. C. Walker, A. T. Boothroyd, D. Prabhakaran, S. P. Collins, and D. F. McMorrow, *J. of Phys.: Condens. Matt.* **24**, 312202 (2012).
- [17] C. Kittel, *Phys. Rev* **82**, 565 (1951).

- [18] R. Khymyn, I. Lisenkov, V. S. Tiberkevich, A. N. Slavin, and B. A. Ivanov, arXiv:1511.05785v3 [cond-mat.mes-hall], (2015).

## Figure Captions:

**Figure 1:** (a) Temperature dependence of  $\text{Sr}_3\text{Ir}_2\text{O}_7$  resistance at small biases ( $I = 0.1$  mA). Open triangles show experimental data, black curve – exponential fit assuming a temperature-dependent activation energy. The (top-right) inset shows the corresponding Arrhenius plot –  $\ln(R)$  vs  $1/T$ . The (bottom-left) inset shows a schematic of our experiment: an electrical current flows between metal contacts (gray) across  $\text{Sr}_3\text{Ir}_2\text{O}_7$  crystal (dark) primarily along the  $[001]$  c-axis. (b) Temperature dependence of the activation energy extracted from the slope of Arrhenius plot. (c) Bias dependence of the activation energy at  $T = 176$  K reconstructed from Arrhenius plots at different biases (not shown).

**Figure 2:** (a) dependence of  $\text{Sr}_3\text{Ir}_2\text{O}_7$  resistance  $R=V/I$  on the bias current  $I$  at different temperatures from 87-180 K (open squares). Solid curves are the field-effect model (Eq. 1) fits. (b-d) Temperature dependences of the model parameters  $A$ ,  $\Delta_0$ , and  $B$ .

**Figure 3:** (a) Reversible resistive switching in  $R(I)$  characteristic of  $\text{Sr}_3\text{Ir}_2\text{O}_7$  ( $T = 77$  K). Gray and black traces represent the up- and down-sweeps of  $I$ . A larger (at  $I_c=\pm 12.7$  mA) and smaller (at  $I_c=\pm 23$  mA) switching events are clearly visible. (b) Switching current  $|I_c|$  vs magnetic field extracted from  $R(I)$ s measured at different fields (not shown). (c) Magnetoresistance of  $\text{Sr}_3\text{Ir}_2\text{O}_7$  at 77 K. Horizontal lines in (b-c) are guides to eye.

**Figure 4:** Effects of microwave irradiation on  $V_\omega(I)$  (left panels) and  $R(I)$  (right panels) characteristics of  $\text{Sr}_3\text{Ir}_2\text{O}_7$ . Gray and black traces show up- and down-sweeps of  $I$ , respectively, for low (-20 dBm – a and b), intermediate (10 dBm – c and d), and high (20 dBm – e and f) power of applied microwaves at 3 GHz.

**Figure 5:** Power dependence of microwave-induced changes in (a)  $R(I)$  and (b)  $V_\omega(I)$ . The power of 3 GHz microwaves is increased from 0-19 dBm in 1 dBm step. Only down-sweeps of  $R(I)$  and  $V_\omega(I)$  are shown (shifted vertically for clarity). The inset shows the critical power  $P_c$  where the resonance-like structure emerges as a function of the frequency of applied microwaves.

**Figure 6:** 2D gray-density plot of the rectification voltage  $V_\omega$  as a function of bias current  $I$  and power  $P$  of 3 GHz microwaves. A brighter (darker) color corresponds to a higher (lower)  $V_\omega$ .

Figure 1:

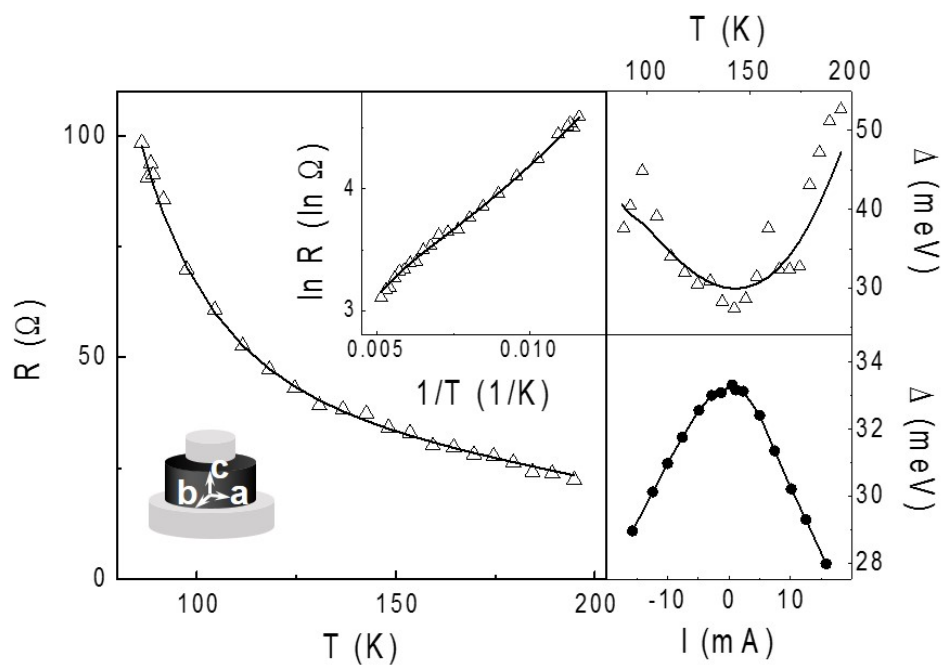


Figure 2:

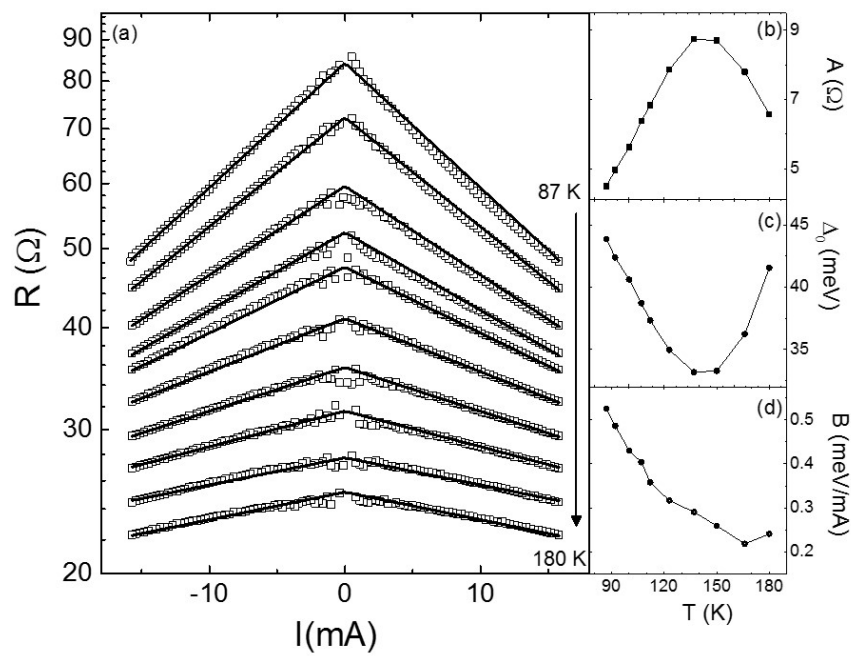


Figure 3:

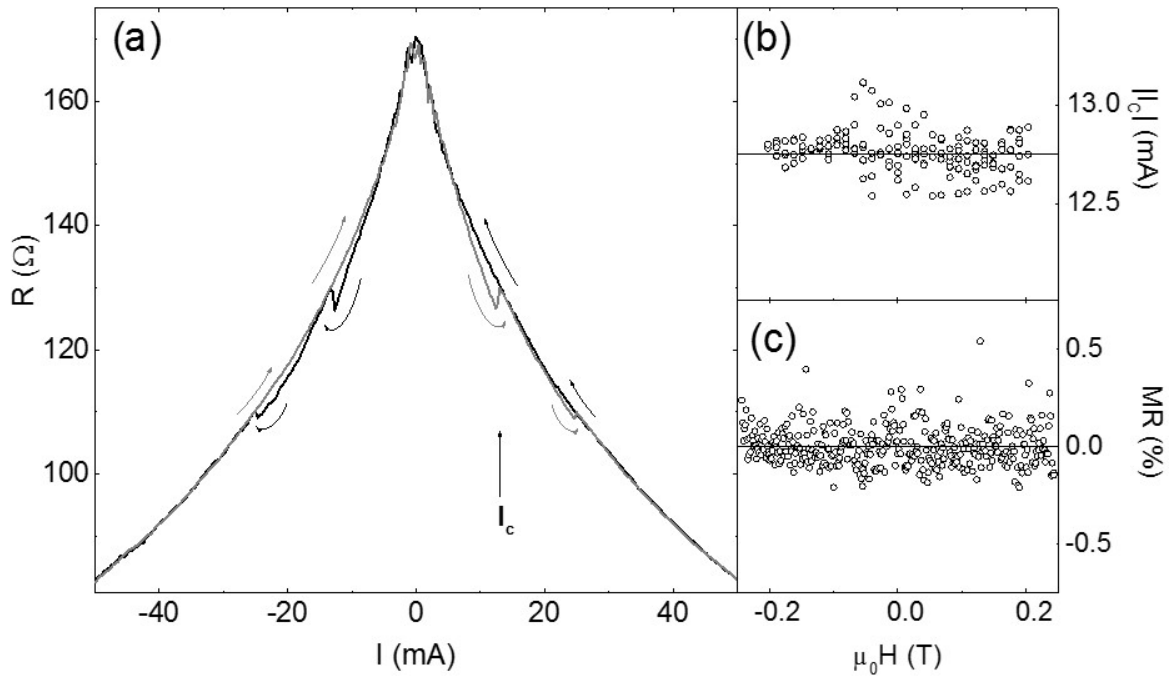
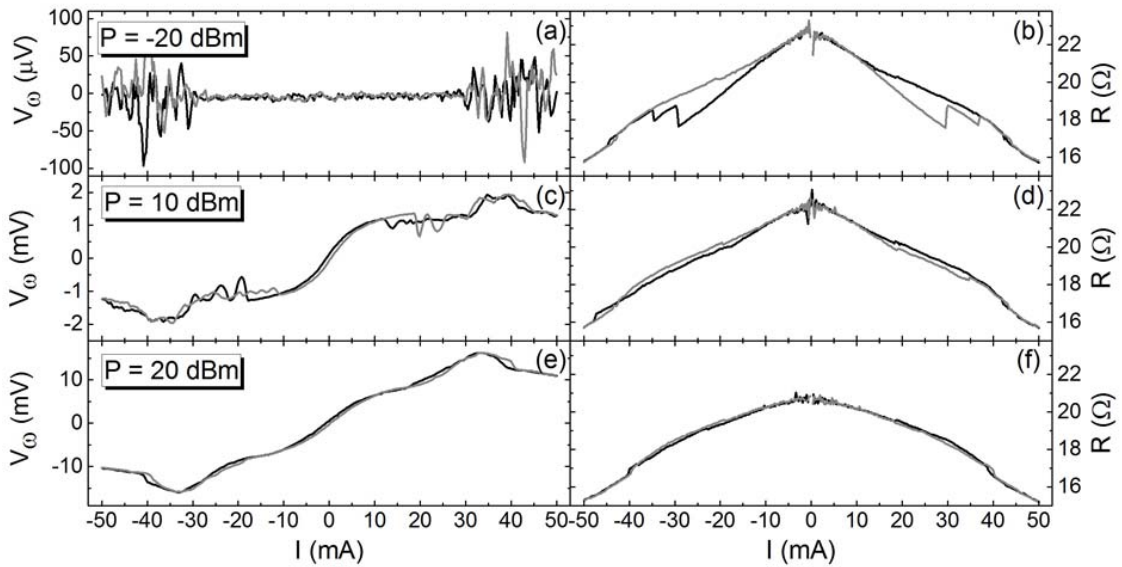
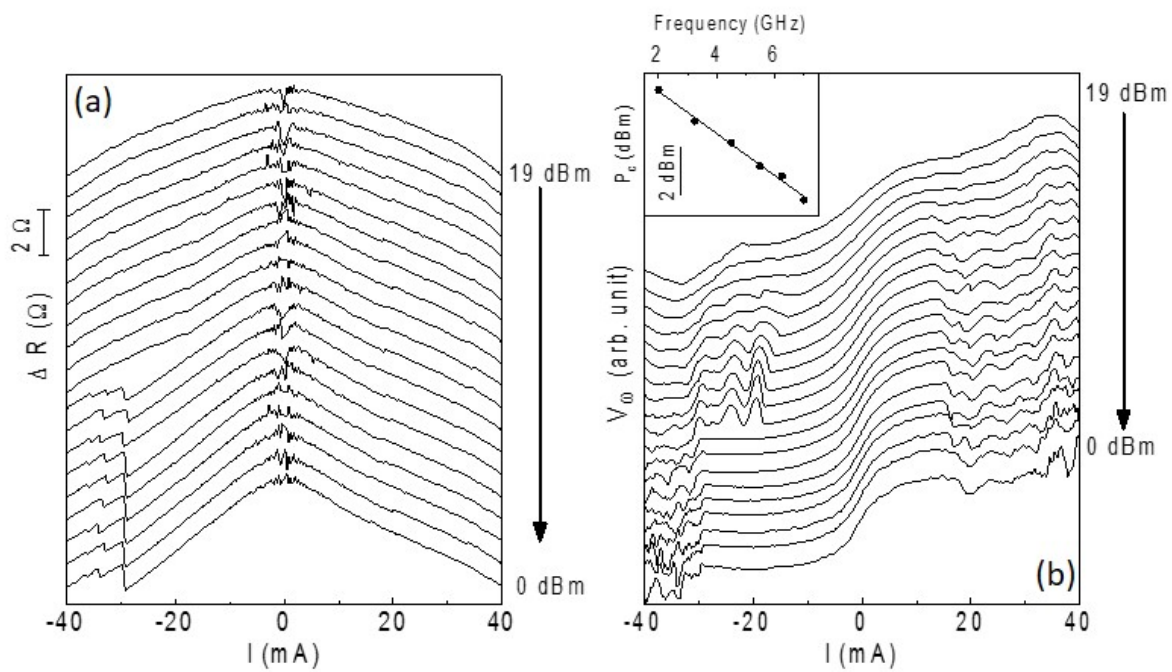


Figure 4:



**Figure 5:**



**Figure 6:**

